Generating and characterising single- and multi-gene mutants of the Rubisco small subunit family in Arabidopsis

Panupon Khumsupan[1], Marta A. Kozlowska[1], Douglas J. Orr[2], Andreas I. Andreou[1], Naomi Nakayama[1], Nicola Patron[3], Elizabete Carmo-Silva[2], Alistair J. McCormick[1,†]

[1]SynthSys & Institute of Molecular Plant Sciences, School of Biological Sciences, University of Edinburgh, Edinburgh, EH9 3BF, UK

[2]Lancaster Environment Centre, Lancaster University, Lancaster, LA1 4YQ, UK.

[3]Earlham Institute, Norwich Research Park, Norwich, NR4 7UZ, UK.

[†]corresponding author:

Dr Alistair J. McCormick
Daniel Rutherford Building

SynthSys and Institute of Molecular Plant Sciences

School of Biological Sciences
University of Edinburgh

The King's Buildings

EH9 3BF

Phone: +44 (0)1316505316

Email: alistair.mccormick@ed.ac.uk

ORCID: 0000-0002-7255-872X
ResearcherID: B-1558-2008

Highlight: A CRISPR/Cas9 approach combined with available T-DNA insertion lines to generate and characterise a suite of single and novel multiple gene knockout mutants of the small subunit family in Arabidopsis.

Abstract

The primary CO_2-fixing enzyme Rubisco limits the productivity of plants. The small subunit of Rubisco (SSU) can influence overall Rubisco levels and catalytic efficiency, and is now receiving increasing attention as a potential engineering target to improve the performance of Rubisco. However, SSUs are encoded for by a family of nuclear *rbcS* genes in plants, which makes them challenging to engineer and study. Here we have used CRISPR/Cas9 and T-DNA insertion lines to generate a suite of single and multiple gene knockout mutants for the four members of the *rbcS* family in Arabidopsis, including two novel mutants *2b3b* and *1a2b3b*. *1a2b3b* contained very low levels of Rubisco (*ca*. 3% relative to WT) and is the first example of a mutant with a homogenous Rubisco pool consisting of a single SSU isoform (1B). Growth under near-outdoor levels of light demonstrated Rubisco-limited growth phenotypes for several SSU mutants and the importance of the 1A and 3B isoforms. We also identified *1a1b* as a likely lethal mutation, suggesting a key contributory role for the least expressed 1B isoform during early development. The successful use of CRISPR/Cas here suggests this is a viable approach for exploring the functional roles of SSU isoforms in plants.

Key words: *Arabidopsis thaliana*, chloroplast, CRISPR/Cas9, photosynthesis, protoplasts, Rubisco, SpCas9, T-DNA

Introduction

Ribulose 1,5-bisphosphate carboxylase/oxygenase (Rubisco, EC 4.1.1.39) catalyses the reaction between CO_2 and ribulose-1,5-bisphosphate (RuBP) and is responsible for net carbon gain in all oxygenic photosynthetic organisms including plants. Despite its importance, Rubisco is a relatively slow and error-prone enzyme that limits the efficiency of photosynthesis. This phenomenon is particularly evident in C3 crop plants, where increasing the operating efficiency of Rubisco and reducing photorespiration are considered promising strategies for improving growth and productivity (Rae et al., 2017; Kubis and Bar-Even, 2019; Simkin et al., 2019; South et al., 2019). In plants, Rubisco (Form IB) is composed of eight large subunits (LSUs) and eight small subunits (SSUs) that form an L_8S_8 complex (Bracher et al., 2017). The LSU is encoded for by a single, highly conserved gene on the chloroplast genome (*rbcL*), while SSUs are encoded by a family of nuclear *rbcS* genes that show significantly more diversity between species compared to *rbcL*. The size of the SSU family also differs between species, with up to twenty isoforms reported in cultivated polyploid wheat varieties (Sasanuma, 2001).

In Form I Rubisco, the eight LSUs form dimers that carry two active sites per dimer. The SSUs are located distal to the active sites and are not required for carboxylation, but are essential to maximise Rubisco activity and are thought to provide structural stability to the L_8S_8 complex (Andersson and Backlund, 2008; van Lun et al., 2011). A substantial body of work in the green alga *Chlamydomonas reinhardtii*, cyanobacteria and higher plants has demonstrated that directed mutagenesis of the SSU, or expression of heterologous SSUs, can significantly modify the catalytic properties of Rubisco, including the turnover rate (k_{cat}), CO_2/O_2 specificity ($S_{c/o}$) and the ability to assemble the L_8S_8 complex (Schneider et al., 1990; Paul et al., 1991; Read and Tabita, 1992; Kostov et al., 1997; Getzoff et al., 1998; Spreitzer et al., 2005; Genkov and Spreitzer, 2009; Ishikawa et al., 2011; Esquivel et al., 2013; Whitney et al., 2015; Atkinson et al., 2017; Fukayama et al., 2019; Orr et al., 2019). More recently, several native, specialised SSU isoforms have been shown to enhance the catalytic properties of Rubisco in plants (Morita et al., 2014; Laterre et al., 2017; Pottier et al., 2018; Lin et al., 2019). This suggests that SSUs naturally play a role in modifying Rubisco performance and thus could be an important target for crop improvement.

The expression levels of SSUs also play a key role in regulating Rubisco abundance, and thus affect whole plant nitrogen and carbon partitioning, and the overall capacity for

carbon uptake (Rodermel, 1999). Previous work has shown that reducing SSU content by antisense RNA or T-DNA insertion results in a decrease in *rbcL* mRNA translation, and subsequently, a decrease in Rubisco content (Rodermel et al., 1996; Wostrikoff and Stern, 2007; Izumi et al., 2012; Ogawa et al., 2012; Wostrikoff et al., 2012; Atkinson et al., 2017). The transcript abundances of SSU families have been explored in detail only for a small number of plant species, such as tomato, wheat, rice and Arabidopsis (Wanner and Gruissem, 1991; Galili et al., 1992; Suzuki et al., 2009; Izumi et al., 2012). Within a species, the strength of promoters for each SSU can vary significantly, resulting in a range of expression levels between different SSU isoforms. Furthermore, expression levels of individual SSUs can vary depending on tissue type and developmental stage, and in response to the growth environment (Wehmeyer et al., 1990; Meier et al., 1995; Ewing et al., 1998; Day et al., 2000; Morita et al., 2014; Laterre et al., 2017). Functional studies for individual SSUs in a species are challenging due to the high sequence homology between SSU isoforms within a family (Yamada et al., 2019). Nevertheless, a better understanding of how the expression of different SSU isoforms is co-ordinated in response to the environment could lead to novel strategies to improve plant growth performances (Cavanagh and Kubien, 2014).

The model plant *Arabidopsis thaliana* (hereafter Arabidopsis) has four SSU genes, *rbcS1A*, *rbcS1B*, *rbcS2B* and *rbcS3B* (hereafter *1A*, *1B*, *2B* and *3B*, respectively), which are divided into A and B subfamilies based on linkage and sequence similarities (Krebbers et al., 1988; Schwarte et al., 2011). *1A* and *3B* are typically reported as the dominant SSU isoforms, while *1B* and *2B* are expressed at lower levels (Izumi et al., 2012; Klepikova et al., 2016). The Arabidopsis SSU family show signs of spatially overlapping and distinct expression during early leaf development (Sawchuk et al., 2008). Although the response of Arabidopsis SSUs to environmental stimuli is relatively well studied (Dedonder et al., 1993; Cheng et al., 1998; Yoon et al., 2001; Sawchuk et al., 2008), a clear understanding of their impact on growth and performance is still lacking.

Gene knockout (KO) mutants generated by T-DNA insertion have been useful tools for functional studies in Arabidopsis (Izumi et al., 2012; Atkinson et al., 2017), but this approach does have limitations. Firstly, T-DNA insertion sites are prone to small deletions, duplications, and filler sequence of unknown origin, while T-DNA lines have been shown to contain chromosomal translocations, and in some cases significant chromosomal rearrangements (Nacry et al., 1998; Clark and Krysan, 2010). Thus, multiple T-DNA insertion lines for a given gene are typically required to verify experimental findings.

However, in some cases only a limited number of T-DNA lines are available for a given locus. Secondly, generating multiple gene knockout lines is time consuming and not feasible for genes with loci in close proximity, as is the case for the three SSU B subfamily gene which, in Arabidopsis, are in a tandem array on chromosome 5 (Krebbers et al., 1988; Niwa et al., 1997).

To overcome this challenge, we have utilised a pooled clustered regularly interspaced short palindromic repeat (CRISPR)/CRISPR-associated protein 9 (Cas9) approach and available T-DNA insertions lines to generate a novel suite of *rbcs* mutants. We produced new single *rbcs* mutants for all four *rbcS* genes, a double *rbcs* mutant (*2b3b*) and a triple *rbcs* mutant (*1a2b3b*). Molecular characterisations were performed to examine the impact of specific SSU mutations on protein and Rubisco contents, while physiological analysis under near-outdoor light levels (1,000 µmol photons m^{-2} s^{-1}) provided novel insights into the contributions of different SSU isoforms to growth performance. This study serves as a proof of principle for future studies to examine the roles of different SSU isoforms in other species.

Materials and Methods

Plant material and growth conditions

Arabidopsis (*Arabidopsis thaliana* (L.) Heyn. Col-0) seeds were sown on soil and stratified for 3d at 4 °C and grown at 22 °C, ambient CO_2, 70% relative humidity and a photosynthetic photon flux (PPFD) of 200 µmol photons m^{-2} s^{-1} (standard lab conditions) or 1,000 µmol photons m^{-2} s^{-1} (high light) supplied by cool white fluorescent lamps (Percival SE-41AR2, Clf Plantclimatics GmbH) in 12:12 light:dark. For comparison of different genotypes, plants were grown from seeds of the same age and storage history, harvested from plants grown in the same environmental conditions. Arabidopsis T-DNA insertion lines *1a* [GABI_608F01 (At1g67090)], *1b* [SAIL_755_D09 (At5g38430)], *2b* [GABI_324A03 (At5g38420)] and *3b* [SALK_117835 (At5g38410)] were sourced from the Nottingham Arabidopsis Stock Centre (NASC). The *1a2b* mutant (GABI_608F01; GABI_324A03) generated previously (Atkinson et al., 2017) was backcrossed with a wild-type plant to remove potential background mutations. The *1a3b* mutant (GABI_608F01; SALK_117835) was provided by Hiroyuki Ishida, Department of Applied Plant Science, Tohoku University, Japan. Homozygous T3 seed stocks for mutants generated via CRISPR/Cas9 in this study can be obtained through the

Nottingham Arabidopsis Stock Centre (http://arabidopsis.info) (NASC IDs N2109789 – N2109802).

Construction of CRISPR/Cas9 vectors

Plasmid vectors were assembled using the Plant MoClo Golden Gate modular cloning kit (Engler et al., 2014). New Level 0 parts were made according to Patron et al. (2015). Level 0 vectors (100 ng each) carrying the UBI10 promoter, the SpCas9 coding sequence (Parry et al., 2016) or the heat shock protein (HSP) terminator (Nagaya et al., 2010) were assembled into the Level 1 Position 2 (L1P2) acceptor vector in a 20 µl assembly reaction (BsaI (ThermoFisher Scientific, UK) (10U), 1X Buffer G, T4 DNA ligase (ThermoFisher Scientific) (400 U), 20 nmol ATP] as in Vasudevan et al. (2019). PCR amplicons of each complete gRNA (the spacer fused to the RNA scaffold) were combined with a Level 0 vector carrying the U6 promoter for assembly (Table S1). Each pair of gRNA expression cassettes were constructed in L1P3 and L1P4, respectively, as described in Raitskin et al. (2019). Four Level 1 transcriptional units (the pFAST selection marker (Shimada et al., 2010) in L1P1, L1P2, L1P3 and L1P4) were then assembled into a Level 2 acceptor vector in a 20 µl assembly reaction [BpiI (ThermoFisher Scientific) (10U), 1 X Buffer G (ThermoFisher Scientific), T4 DNA ligase (ThermoFisher Scientific) (400 U) and 20 nmol of ATP] (see Data S1) as in Vasudevan et al. (2019).

DNA and RNA extraction, PCR and RT-qPCR

DNA was extracted from a mature leaf as described in Li and Chory (1998). PCR reactions were performed as in McCormick and Kruger (2015) using gene-specific primers (Table S2). Total RNA was isolated from leaves using the RNeasy plant mini kit (Qiagen, USA). Isolated RNA was treated with DNase (Qiagen) and reverse transcribed with random primers (Promega, USA). Gene-specific primers amplifying the unique 3' region of the transcript were used for RT-qPCR (Izumi et al., 2012). A DNA fragment containing regions matching the target loci of the *rbcS* for RT-qPCR primers was synthesised (Gblock, IDT) (Fig. S1). RT-qPCR calibration curves were constructed using known concentrations of the standard to quantify mRNA levels for each *rbcS* transcript pool. For quantitative analysis, an aliquot of

cDNA derived from 4 ng of RNA was used (total volume 20 µl) with SYBR Green Master Mix (Eurogentec, Belgium).

CRISPR/Cas9 cassettes in protoplasts

Leaves from 4-week-old plants were cut vertically into 1 mm strips and digested in 10 ml maceration glycine glucose (MGG) digestion solution as in Chupeau et al. (2013) containing cellulase "Onozuka" R-10 (1.5% [w/v]) and Macerozyme R-10 (0.4% ([w/v]) (Yakult Pharmaceutical, Japan) for 3 h. Released protoplasts were filtered from the digestate using a 70 µm cell strainer and washed three times with MGG not containing enzymes to remove traces of the enzyme solution and cell debris. Protoplasts were resuspended in MMM solution (0.4 M mannitol, 15 mM $MgCl_2$, 0.1% [w/v] MES [pH 8]) to a concentration of 5 x 10^5 cells ml^{-1} in a 5 ml glass test tube. For protoplast transformations, 8 µl DNA (4 µg total) was added to 75 µl of the protoplast suspension, followed by addition of 83 µl of PEG solution (0.4 M mannitol, 0.1 M $Ca(NO_3)_2.4H_2O$, 40% [w/v] PEG 4000 [pH 8]). Following a 1 min incubation, 2 ml of MGG solution was added. Following a further 1 hr incubation at RT, the protoplasts were centrifuged at 70 *g* for 5 min and the supernatant removed. Fresh MGG solution was added (100 µl) and transfected protoplasts were incubated in the dark for 18 h at RT. The target loci of each CRISPR/Cas9 vector was analysed by PCR of protoplast DNA extracts (Table S2).

Expression of Cas9 and gRNA in Arabidopsis

Binary vectors (Level 2) were transformed into *Agrobacterium tumefaciens* (AGL1) for stable insertion in Arabidopsis by floral dipping (Clough and Bent, 1999). T1 plants were screened for the presence of the transgene by the pFAST selectable marker (Shimada et al., 2010), and for the presence of CRISPR/Cas9-mediated mutations by PCR and Sanger sequencing (Table S2). Stable mutations in transgene-free T2 plants were confirmed by Sanger sequencing.

Protein quantification and Rubisco content

Leaf samples (20-40 mg) were collected from 35-d-old plants, snap frozen and stored at -80 °C prior to extraction. Samples were ground rapidly in an ice-cold mortar and pestle in 200 µl of protein extraction buffer (50 mM Bicine-NaOH pH 8.2, 20 mM $MgCl_2$, 1 mM EDTA, 2 mM benzamidine, 5 mM ε-aminocaproic acid, 50 mM 2-mercaptoethanol, 10 mM dithiothriotol, 1% [v/v] protease inhibitor cocktail [Sigma-Aldrich, USA], and 1 mM phenylmethylsulphonyl fluoride) for *ca*. 1 min followed by centrifugation at 14,700 *g* at 4 °C for 1 min. Supernatant (90 µl) was then mixed with 100 µl of carboxyarabintol-1,5-bisphosphate (CABP) binding buffer (100 mM Bicine-NaOH [pH 8.2], 20 mM $MgCl_2$, 20 mM $NaHCO_3$, 1.2 mM [37 kBq/µmol] [^{14}C]CABP), incubated at RT for 25 min, and Rubisco content determined via [^{14}C]CABP binding (Sharwood et al., 2016). Bradford assay was used to determine total soluble protein in the same supernatant as prepared for Rubisco content analysis (Bradford, 1976).

Extracts were subjected to SDS-PAGE on a 4-12% (w/v) polyacrylamide gel (Bolt® Bis-Tris Plus Gel) (ThermoFisher Scientific, UK), transferred to PVDF membrane then probed with rabbit serum raised against wheat Rubisco at 1:10,000 dilution (Howe et al., 1982) followed by LI-COR IRDye® 800CW goat anti-rabbit IgG (LI-COR Biosciences, USA) at 1:10,000 dilution, then viewed on an LI-COR Odyssey CLx Imager. The relative abundance of LSU and SSUs were estimated densitrometically using Image Studio Lite (LI-COR Biosciences) and the values were means ± SE based on three immunoblots as in Atkinson et al. (2017)

Chlorophyll quantification

Leaf discs (20 mm^2 in total) were frozen in liquid N_2, powdered, and then mixed with 1 ml of ice-cold 80% (v/v) acetone, 10 mM Tris-HCl. Following centrifugation at 17,200 *g* for 10 min, chlorophyll was quantified according to Porra et al. (1989).

Measurement of photosynthetic parameters

Gas exchange and chlorophyll fluorescence were determined using a LI-COR LI-6400 portable infra-red gas analyser (LI-COR Biosciences) with a LI6400-40 leaf chamber (2 cm^2 area) on either the sixth or seventh leaf of 35- to 45-d-old rosettes grown under 200 µmol photons m^{-2} s^{-1} in large pots to generate leaf area sufficient for gas exchange measurements (Atkinson et al., 2017). For all gas exchange experiments, leaf temperature and chamber relative humidity were 25 °C and *ca*. 65%, respectively. The response of *A* to the intercellular CO_2 concentration (C_i) was measured at various CO_2 concentrations (50, 100, 150, 200, 250, 300, 350, 400, 500, 700, 900 and 1,200 µmol mol^{-1}) under saturating light (1,800 µmol photons m^{-2} s^{-1}) (Fig. S2). Gas exchange data were corrected for CO_2 diffusion from the measuring chamber as in Bellasio et al. (2016). To calculate the maximum rate of Rubisco carboxylation (V_{cmax}), the *A*/*C*i data were fitted to the C_3 photosynthesis model as in Ethier and Livingston (2004) using the catalytic parameters K_c^{air} and affinity for O_2 (K_o) values for wild-type Arabidopsis Rubisco at 25 °C from Atkinson et al. (2017). Estimates of the light- and CO_2-saturated photosynthetic electron transport rate (J_{max}) were not included as several of the SSU mutants were likely Rubisco-limited even at high CO_2 concentrations. Maximum quantum yield of photosystem II (PSII) (F_v/F_m) was measured using a Hansatech Handy PEA continuous excitation chlorophyll fluorimeter (Hansatech Instruments, UK) (Maxwell and Johnson, 2000).

Rosette area and biomass

Rosettes were imaged daily during growth experiments. Rosette area was calculated using iDiel Plant software (Dobrescu et al., 2017). For biomass measurements, aerial rosette tissue was removed and weighed to determine fresh weight. Samples were then dried in an oven (80 °C for 3 d) and weighed to determine dry weight.

Statistical analysis

Significant differences between sample groups were assessed by one-way analysis of variance (ANOVA) followed by Tukey's honest significant difference (HSD) post hoc test (IBM SPSS Statistics Ver. 26.0, USA) for individual parameters. Difference in growth performance (as measured by rosettes area) were assessed by repeated measures ANOVA followed by Tukey's HSD post hoc test.

Results

Identification of T-DNA insertion lines and double knockout mutants

We initially performed a search for available Arabidopsis mutant lines on T-DNA Express (http://signal.salk.edu/cgi-bin/tdnaexpress) that carry a single homozygous T-DNA insertion, ideally located in exonic regions for members of the SSU gene family. We identified only one such line for *1A* (GABI_608F01) and *2B* (GABI_324A03) (Fig. 1A). The only available homozygous mutants for *1B* (SAIL_755_D09) and *3B* (SALK_117835) had insertion sites located in the 5' UTR. For the latter, *3B* expression is reportedly reduced but not absent (Izumi et al., 2012).

Double mutants *1a2b* and *1a3b* were generated previously by crossing available T-DNA lines (Izumi et al., 2012; Atkinson et al., 2017). Upon further characterisation of *1a2b*, we observed that the mutant had a defective silique phenotype, with a reduced silique size and seed count per silique (Fig. S3A, S3B). Backcrossing with a wild-type (WT) plant and then re-segregating *1a2b* in the F2 generation removed the observed silique phenotype, indicating that this trait was not attributable to the absence of 1A and 2B. Furthermore, the new *1a2b* showed a more robust growth phenotype compared to the original double mutant (Fig. S3C). Single *rbcs* mutant lines for *1a* or *2b* did not show a silique phenotype. We identified plants in the segregating F2 population with the silique phenotype or reduced growth, but with no T-DNA insertions in either *1A* or *2B*, indicating that these traits were possibly linked to a recessive heterozygous mutation in either the *1a* or *2b* parental line. The new *1a2b* double mutant was used for the remainder of this study. We also attempted to generate a *1a1b* double mutant by crossing the T-DNA insertion mutants for *1a* and *1b*, and were successful in generating a heterozygote F1 (1A*1a*1B*1b*) line (Fig. S4). We were not able to recover a *1a1b* mutant after screening 125 F2 plants, but did identify a 1A*1a1b1b* line.

Analysis of 15 F3 progeny of the latter line failed to show a Mendelian distribution for the *1A* locus (8: 7: 0; WT: heterozygous: homozygous KO), suggesting that *1a1b* may be lethal. The germination rates of seeds recovered from the mutant lines were comparable to WT plants (WT = 93%, 1A*1a*1B*1b* = 93%, 1A*1a1b1b* = 96% of *ca*. 100 seeds), indicating that selection against a *1a1b* genotype occurred prior to seed development.

gRNA targeting strategy and transient expression of Cas9/gRNAs in protoplasts

To generate new *rbcs* mutants for individual members of the Arabidopsis SSU family using the CRISPR/Cas9 method, we initially designed two unique pairs of guide RNAs (gRNAs) to target specific regions of each of the four *rbcS* genes, for a total of eight gRNA pairs (Fig. 1A; Table S1). Furthermore, to knock out *1B*, *2B* and *3B* simultaneously we designed a promiscuous pair of gRNAs to target homologous regions in the *1B-3B* locus (Fig. 1B; Table S1). A paired gRNA approach was chosen for two reasons: i) to increase the probability of generating mutations and ii) the generation of larger deletions between the two gRNAs could potentially be screened more easily and cheaply (e.g. by PCR). Each gRNA pair was assembled using the Plant MoClo system as an individual expression cassette in a Level 2 binary vector containing a Cas9 expression cassette (Data S1) (Engler et al., 2014).

Vectors with each *rbcS* specific gRNA pair were initially tested using a novel Arabidopsis protoplast transient expression system to estimate the efficiency of generating deletion events (Fig. 2A). Following transfection of the gRNA pairs targeting *1A* or *1B*, amplification of the respective gene loci produced the expected WT band and a second lower band indicating a deletion event based on the target sites of the gRNA pair. Pairs 1AP2 and 1BP2 most consistently produced prominent "deletion bands" for *1A* and *1B*, respectively, and thus were selected for *in planta* expression. Only one gRNA pair each for *2B* (2BP2) and *3B* (3BP1) produced a deletion band. Sequence analysis of the deletion bands indicated cleavage 3-4 bp downstream of the gRNA PAM sites, consistent with the activity of SpCas9, and deletions ranging from 96 bp to 180 bp (Fig. 2B).

Expression of CRISPR/Cas9 in planta to generate stable mutants for each rbcS isoform

Arabidopsis plants were stably transformed with CRISPR/Cas9 binary vectors containing gRNA pairs 1AP2, 1BP2, 2BP2, 3BP1 and the promiscuous pair 1B3B. Transformed T1 seeds were visually selected using the pFAST red fluorescent seed coat marker for the presence of Cas9 and gRNAs (Shimada et al., 2010). The loci of the five gRNA pairs were initially screened by PCR for large deletions, which were detected in transformants for 1AP1, 2BP2 and 3BP1 but not for 1BP2 (Fig. S5A). The deletion bands were consistent with those observed in protoplasts (Fig. 2A). Several deletion bands were detected for 1B3B that were consistent with predicted amplicon sizes following multiple cleavage events within the *1B-3B* locus (Fig. S5B). Sequencing of each amplicon showed the expected cleavage position downstream of the PAM sites.

The efficiency with which deletions were induced by gRNA pairs ranged from 1-14% (Table 1). However, all deletions that were detected were accompanied by a significantly brighter WT band, indicating chimeric rather than heritable genomic mutations (i.e. homozygous or heterozygous) (Feng et al., 2014; Pauwels et al., 2018). T1 transformants were also screened by Sanger sequencing to detect potential small indel mutations at each gRNA target site (Fig. S5C). Indels were generally detected at a higher frequency than large deletions (3-31%).

Screening for heritable mutations in the T2 generation was performed on segregated non-red seed progeny (i.e. containing no CRISPR/Cas9 insertion). Eight progeny from each T1 line that showed large deletions were screened by PCR (Table 1). No heritable large deletions were detected for any gRNA pair, confirming that the observed deletions in T1 were chimeric mutations. Sanger sequencing was then performed on T2 lines that contained large deletions or indels in T1. Stable homozygous indels (i.e. frame-shift mutations in exonic regions that produced early stop codons) were identified for all four *rbcS* genes targeted by specific gRNA pairs (Table S3; Fig. S6). For the promiscuous gRNA pair 1B3B, each of the B subfamily genes was sequenced in 64 non-red T2 plants from eight T1 lines showing large deletions. No mutations were observed in *1B* in any of the lines tested. However, we did identify a 147 bp deletion in *3B* common to the progeny of a single T1 line. Sequencing of the eight progeny revealed an additional 4 bp indel deletion in *2B* in a single plant, thus producing a *2b3b* double mutant. For *2b3b*, both indels led to frame-shift mutations that produced early stop codons in *2B* and *3B*. For all *rbcs* lines, T2 plants containing

homozygous mutations were selected and seeds were collected for subsequent molecular and physiological characterisations in the T3 generation.

Generating triple rbcs mutants using the 1a2b T-DNA insertion mutant

We next introduced CRISPR/Cas9 binary vectors containing gRNA pairs 3BP1 or 1BP2 into the new *1a2b* double T-DNA insertion mutant to attempt to produce the novel triple mutants *1a2b3b or 1a1b2b*. Out of 30 T1 *1a2b* transformants for 3BP1, three showed a slow-growth, pale leaf phenotype compared to the *1a2b* phenotype (Table 1; Fig. 3A). Sanger sequencing of the *3B* locus confirmed the presence of a homozygous and biallelic frame-shift mutation in all three T1 plants (Fig. S6). The heritability of those mutations was confirmed in non-red seed progeny of the T2 generation for each line. In contrast, 1B is a minor SSU isoform, so no growth phenotype was expected in T1 *1a2b* transformants for 1BP2. Sanger sequencing of the *1B* locus in 33 T1 plants showed mutations in *1B* for eight plants (*ca*. 25%) indicating that the CRISPR/Cas9 was functional and efficient. However, in all cases only single bp changes (i.e. a single codon substitution) or silent substitutions were observed (Fig. S7).

Molecular characterisation of rbcs mutants

The expression profiles of the *rbcS* family and *rbcL* were quantified in T3 plants for each *rbcS* mutant line. Transcript abundances were generally reduced for *rbcS* genes in lines targeted by specific T-DNA insertions or CRISPR/Cas9 editing (Table S4). Consistent with previous observations, the relative expression of *rbcL* was more repressed in mutants with greater reductions in overall *rbcS* expression (i.e. *1a3b* and *1a2b3b*) (Wostrikoff and Stern, 2007; Izumi et al., 2012; Wostrikoff et al., 2012; Atkinson et al., 2017).

The total soluble protein content in leaves of all single mutants, and double mutants *1a2b* and *2b3b*, was similar to that of WT plants, but was significantly reduced by 20% and 82% for *1a3b* and *1a2b3b*, respectively (Fig. 3B, Table S5). Leaf Rubisco content was generally decreased in single *rbcS* mutants compared to WT plants, and was significantly reduced in all double mutants and *1a2b3b* (Fig. 3C). Specifically, *1a2b* and *2b3b* had Rubisco levels reduced by 42% and 38%, respectively, *1a3b* by 61% and *1a2b3b* by 97% relative to WT plants. Disruption of *1A* led to an absence of the lower 1A SSU (14.7 kDa)

band in *1a*, *1a2b*, *1a3b* and *1a2b3b* mutants as detected by Western blot (Fig. 3D). Similarly, disruption of *3B* resulted in a reduction in the intensity of the upper SSU band of the B-subfamily genes (14.8 kDa) in *3b*, *2b3b*, *1a3b* and *1a2b3b* mutants. In contrast, no observable reductions in upper band intensity were observed with mutants of the less expressed isoforms *1B* and *2B*. Nevertheless, the SSU band intensity of *1a2b3b* was 30-fold lower than that of the overall intensity of the WT SSU bands.

Characterisation of rbcs mutants under normal light and high light

Growth assays were performed under standard lab conditions for Arabidopsis plants (i.e. PPFD = 200 µmol photon m^{-2} s^{-1}) and under near-outdoor levels of light (i.e. PPFD = 1,000 µmol photon m^{-2} s^{-1}) to characterise the growth performance of the *rbcs* mutants. Under standard lab conditions, the gene knockout mutants for individual *rbcS* genes generated by CRISPR/Cas9 or T-DNA insertion (i.e. *1a*, *1b*, *2b* and *3b*), as well as double mutants *1a2b* and *2b3b*, did not differ from WT plants in terms of rosette expansion rate, fresh weight (FW), dry weight (DW), specific leaf area (SLA), maximum potential quantum efficiency of PSII (F_v/F_m), or chlorophyll content (Fig. 4; Table S6). In contrast, *1a3b* and *1a2b3b* showed significant reductions in area, FW, DW, SLA, chlorophyll content, and F_v/F_m. *1a2b3b* was more slow-growing than *1a3b*, but eventually developed to a similar level under standard lab conditions and produced viable seeds (Fig. 3A).

Under high light, *1a* and all three double mutants had significantly lower area, FW, DW, and chlorophyll content compared to WT. A significant reduction in FW and DW was also observed for *3b* mutants, while rosette area remained similar to WT. As a result, *3b* mutants also had a significantly higher SLA than WT. High light was lethal to the *1a2b3b* triple mutant, which did not survive past 15 days after germination.

The response of A to C_i under saturating light (A/C_i curves) was measured for all *rbcs* mutant lines grown under standard lab conditions (Fig. 5) as well as key photosynthetic variables (Table 2). Stomatal conductance to CO_2 at ambient CO_2 (g_s) and respiration rates in the dark (R_d) were the same in all lines, consistent with previous work showing that reductions in Rubisco do not affect stomatal behaviour or mitochondrial respiration in Arabidopsis (Atkinson et al., 2017). Single *rbcs* mutants for *1A* and *3B* showed significant decreases in the maximum rate of Rubisco carboxylation (V_{cmax}) compared to WT plants. In

contrast, *1b* and *2b* mutants were similar to WT. All three double mutants (*1a2b*, *2b3b* and *1a3b*) had decreased V_{cmax}, and *1a3b* also showed an increased sub-stomatal CO_2 compensation point (Γ). However, *1a2b3b* was significantly different from all other plant lines, with a four-fold higher Γ value, and V_{cmax} at 10% of WT values.

Discussion

Although the uptake of CRISPR/Cas9 in plant biology has increased dramatically in recent years, many aspects concerning efficiency are still unclear, especially as established guidelines for CRISPR/Cas9 in other biological systems are not necessarily applicable to plants (Liang et al., 2016; Hahn and Nekrasov, 2019). As the generation of stable plant transformants is time-consuming, we adopted a more rapid, transient expression approach using Arabidopsis protoplasts to test the efficiency of different gRNA pairs and select robust candidates. All selected gRNA pairs were active in Arabidopsis and resulted in stable *rbcs* mutants. Thus, in agreement with previous studies (e.g. Li et al., 2013; Durr et al., 2018), screening gRNAs in protoplasts appears to be a reliable method for selecting functional gRNAs *in planta*. Overall, CRISPR/Cas appeared a viable approach to examine the impact of mutating *rbcS* isoforms and exploring their functional roles in plants.

CRISPR/Cas9 editing can be utilised to edit closely linked genes, which is not technically feasible through crossing T-DNA insertion lines such as genes in the *rbcS* B-subfamily. Here, the *2b3b* double *rbcs* mutant was successfully generated by targeting homologous regions by the gRNA pair 1B3B. In addition, the triple mutant *1a2b3b* was generated by targeting *3B* in the *1a2b* T-DNA line. Interestingly, disruption of *1B* in conjunction with other *rbcS* genes was not accomplished using T-DNA insertion or CRISPR/Cas9 approaches despite successful generation of *1b* mutants with both methods. 1B is the least expressed *rbcS* isoform and the mature peptide differs from 2B and 3B by only two amino acid residues (Izumi et al., 2012). Thus, it is unlikely that the structure of 1B has a unique impact on Rubisco activity (Valegård et al., 2018). Nevertheless, the temporal and/or spatial expression of 1B may contribute a specialised functional role that is critical for Arabidopsis development or fitness (i.e. during procreation). For example, previous work has shown that 1B localises exclusively to the abaxial side of primordia and young leaves (Sawchuk et al., 2008). It would be interesting to further examine 1B localisation in reproductive tissues (e.g. siliques or flowers). As a product of gene duplication, *1B* is subject

to selection pressure and is not retained in all accessions of Arabidopsis, although loss was correlated with disruption of the promoter (Schwarte and Tiedemann, 2011). Retention of 1B may be linked to sublocalisation (Qiu et al., 2019). Differential expression patterns of *rbcS* genes in different organs have also been observed in other plant species including tomato, maize, tobacco and rice (Wanner and Gruissem, 1991; Ewing et al., 1998; Morita, et al., 2014; Laterre et al., 2017). However, the extent of how important these organ-specific SSUs are has not yet been explored.

Gene editing via CRISPR/Cas9 resulted in a general decrease in mRNA abundance of target genes and significant reductions in Rubisco content for all *1a*, *1a2b*, *1a3b* and *1a2b3b* mutants. The observed reduction in mRNA levels was likely due to the presence of early stop codons that emerged from frame-shift mutations, which consequently led to the degradation of mRNA through the nonsense-mediated decay process (Hug et al., 2015). Reductions in *rbcS* transcripts led to a reduction in the *rbcL* transcript but not to the same extent, as Arabidopsis *rbcL* transcript is controlled post-transcriptionally at the translation initiation process (Rodermel et al., 1996). Similar to Arabidopsis, *rbcL* synthesis in tobacco was shown to be partially independent of the *rbcS* transcript level and LSU production was subject to assembly state-dependent regulation that operated at the translational level (Wostrikoff and Stern, 2007).

rbcs mutants with a relatively small reduction in Rubisco content (i.e. above < 40% of WT levels), showed no change in growth rate and biomass accumulation relative to WT plants under standard lab growth conditions (i.e. PPFD = 200 µmol photons m^{-2} s^{-1}). This was not unexpected as reductions in Rubisco content have previously been shown to be compensated by an increase in activation state of the remaining Rubisco pool under conditions that are non-limiting for Rubisco (Quick et al., 1991). However, under high light conditions (i.e. PPFD = 1,000 µmol photons m^{-2} s^{-1}), biomass accumulation (i.e. FW and DW) was significantly decreased in *1a* and *3b* mutants and all three double mutants (i.e. *2b3b*, *1a2b* and *1a3b*). This demonstrates that under near-outdoor levels of light, both 1A and 3B are critical for normal growth.

Differential expression of the Arabidopsis *rbcS* genes has been observed previously (e.g. under changing temperatures, light qualities and CO_2 concentrations (Dedonder et al., 1993; Cheng et al., 1998; Yoon et al., 2001; Sawchuk et al., 2008)) but the impact of these differences on growth remains unclear. One potential use of our *rbcS* mutant suite could be to

further examine the importance and interaction of specific SSU isoforms during development. All SSUs with the exception of *1B* are increased in response to specific wavelengths of light (i.e. blue, red and far-red light), but at differing relative gene expression levels (Dedonder et al., 1993; Sawchuk et al., 2008). Furthermore, *1A* is the major isoform below 20 °C, whereas *3B* expression is dominant at 30 °C (Yoon et al., 2001; Izumi et al., 2012).

The rosette area of *3b* mutants was not decreased under high light compared to WT plants. However, the observed reduction in biomass resulted in a significant increase in SLA and suggested that leaves were thinner in those lines. Furthermore, gas exchange measurements demonstrated a decrease in V_{cmax} for *3b* mutants. Similar increases in SLA and reductions in photosynthetic capacity were observed for *1a* and all three double mutants. These observations are in line with previous growth analyses of Arabidopsis Rubisco activase antisense lines under high light (Eckardt et al., 1997), where a reallocation of resources to expand leaf area and reduce thickness was observed when photosynthetic capacity was limiting (Hoshino et al., 2019).

For the most severerly Rubisco-limited mutants, *1a3b* and *1a2b3b*, F_v/F_m was reduced under standard light. However, F_v/F_m for *1a3b* was similar to WT under high light, indicating that a reduction in Rubisco has less impact on the operating efficiency of the light reactions under high light. Thus, failure of *1a2b3b* to grow under high light could indicate an inability of the light reactions to co-ordinate product utilisation (i.e. ATP and NADPH) with the extremely low Rubisco content of the triple mutant.

CRISPR/Cas9 is a versatile tool that has been successfully used for genetic editing and the enhancement of breeding strategies in a wide variety of plant and crop species (Khumsupan et al., 2019; Wolter et al., 2019). This study has shown that CRISPR/Cas is a viable approach for characterizing the roles of SSUs in plant species and that Arabidopsis mutants lacking SSU isoforms are useful platforms for the study of functional roles of SSUs. In particular, the triple mutant *1a2b3b* is potentially a powerful resource for studying the impact of heterologous SSU expression that has previously been studied in the *1a3b* background (Atkinson et al., 2017). Unlike *1a3b*, which has a Rubisco content of *ca*. 35% relative to WT (Izumi et al., 2012; Atkinson et al., 2017), *1a2b3b* retained only 3% under the conditions tested, and is the first example of a plant line with a homogenous Rubisco pool consisting of single SSU and a single LSU isoform. Following complementation, further disruption of the remaining *1B* isoform (e.g. by CRISPR/Cas9 editing using gRNA pair

1BP2) could be used to generate a true hybrid Rubisco pool comprised of only heterologous SSU(s) and the native LSU. In addition, as the contribution of individual SSUs to the Rubisco enzyme is still unclear, the triple mutant could be exploited as a model to knock in native SSUs tagged with different fluorescent probes (Ishida et al., 2008). This method would allow for the visualisation of composition of each hexadecamer in the Rubisco enzyme.

Acknowledgments

This work was supported by the UK Biotechnology and Biological Sciences Research Council (grants BB/I024488/1 to E.C-S., and BB/M006468/1 and BB/S015531/1 to A.J.M.), and the Leverhulme Trust (grant RPG-2017-402 to A.J.M.). P.K. was funded by a postgraduate research scholarship from the Darwin Trust of Edinburgh. We thank Louis Caruana (Lancaster University) for technical support.

References

Andersson I, Backlund A. 2008. Structure and function of Rubisco. Plant Physiology and Biochemistry **46**, 275–291.

Atkinson N, Leitão N, Orr DJ, Meyer MT, Carmo-Silva E, Griffiths H, Smith, AM, McCormick AJ. 2017. Rubisco small subunits from the unicellular green alga Chlamydomonas complement Rubisco-deficient mutants of Arabidopsis. New Phytologist **21**, 655–667.

Bellasio C, Beerling DJ, Griffiths H. 2016. An Excel tool for deriving key photosynthetic parameters from combined gas exchange and chlorophyll fluorescence: theory and practice. Plant, Cell and Environment **39**, 1180–1197.

Bracher A, Whitney SM, Hartl FU, Hayer-Hartl M. 2017. Biogenesis and metabolic maintenance of Rubisco. Annual Review of Plant Biology **68**, 29–60.

Bradford MM. 1976. A rapid and sensitive method for the quantitation of microgram quantities of protein utilizing the principle of protein-dye binding. *A*nalytical Biochemistry **72**, 248–254.

Cavanagh AP, Kubien DS. 2014. Can phenotypic plasticity in Rubisco performance contribute to photosynthetic acclimation. Photosynthesis Research **119**, 203–214.

Cheng SH, Moore BD, Seemann JR. 1998. Effects of short- and long-term elevated CO_2 on the expression of ribulose-1,5-bisphosphate carboxylase/oxygenase genes and carbohydrate accumulation in leaves of *Arabidopsis thaliana* (L.) Heynh. Plant Physiology **116**, 715–723.

Chupeau MC, Granier F, Pichon O, Renou JP, Gaudin V, Chupeaua Y. 2013. Characterization of the early events leading to totipotency in an Arabidopsis protoplast liquid culture by temporal transcript profiling. The Plant Cell **25**, 2444–2463.

Clark K, Krysan P. 2010. Chromosomal translocations are a common phenomenon in *Arabidopsis thaliana* T-DNA insertion lines. The Plant Journal **6**, 990–1001.

Clough SJ, Bent AF. 1999. Floral dip : a simplified method for Agrobacterium-mediated transformation of *Arabidopsis thaliana*. The Plant Journal **16**, 735–743.

Czechowski T, Stitt M, Altmann T, Udvardi MK, Scheible WR. 2005. Genome-wide identification and testing of superior reference genes for transcript normalization in Arabidopsis. Plant Physiology **139**, 5–17.

Day CD, Lee E, Kobayashi J, Holappa LD, Albert H, Ow DW. 2000. Transgene integration into the same chromosome location can produce alleles that express at a predictable level or alleles that are differentially silenced. Genes and Development **14**, 2869–2880.

Dedonder A, Rethy R, Fredericq H, Van Montagu M, Krebbers E. 1993. Arabidopsis *RbcS* genes are differentially regulated by light. Plant Physiology **101**, 801–808.

Dobrescu A, Scorza LCT, Tsaftaris SA, McCormick AJ. 2017. A "Do-It-Yourself" phenotyping system: measuring growth and morphology throughout the diel cycle in rosette shaped plants. Plant Methods **13**, 95.

Durr J, Papareddy R, Nakajima K, Gutierrez-Marcos J. 2018. Highly efficient heritable targeted deletions of gene clusters and non-coding regulatory regions in Arabidopsis using CRISPR/Cas9. Scientific Reports **8**, 1–11.

Eckardt NA, Snyder GW, Portis AR, Ogren WL. 1997. Growth and photosynthesis under high and low irradiance of *Arabidopsis thaliana* antisense mutants with reduced ribulose-1,5-bisphosphate carboxylase/oxygenase activase content. Plant Physiology **113**: 575–586.

Engler C, Youles M, Gruetzner R, Ehnert TM, Werner S, Jones JDG, Patron NJ, Marillonnet S. 2014. A Golden Gate modular cloning toolbox for plants. ACS Synthetic Biology **3**, 839–843.

Esquivel MG, Genkov T, Nogueira AS, Salvucci ME, Spreitzer RJ. 2013. Substitutions at the opening of the Rubisco central solvent channel affect holoenzyme stability and CO_2/O_2 specificity but not activation by Rubisco activase. Photosynthesis Research **118**, 209–218.

Ethier GJ, Livingston NJ. 2004. On the need to incorporate sensitivity to CO_2 transfer conductance into the Farquhar-von Caemmerer-Berry leaf photosynthesis model. Plant, Cell and Environment **27**, 137–153.

Ewing RM, Jenkins GI, Langdale JA. 1998. Transcripts of maize *RbcS* genes accumulate differentially in C3 and C4 tissues. Plant Molecular Biology **36**, 593–599.

Feng Z, Mao Y, Xu N, Zhang B, Wei P, Yang DL, Wang Z, Zhang Z, Zheng R, Yang L, Zeng L, Liu X, Zhu J-K. 2014. Multigeneration analysis reveals the inheritance, specificity, and patterns of CRISPR/Cas-induced gene modifications in Arabidopsis. Proceedings of the National Academy of Sciences USA **111**, 4632–4637.

Fukayama H, Kobara T, Shiomi K, Morita R, Sasayama D, Hatanaka T, Azuma T. 2019. Rubisco small subunits of C 4 plants, Napier grass and guinea grass confer C4-like catalytic properties on Rubisco in rice. Plant Production Science **22**, 296–300.

Galili S, Galili G, Avivi Y, Feldman M. 1992. Identification and chromosomal location of four subfamilies of the Rubisco small subunit genes in common wheat. Theoretical and Applied Genetics **83**, 385–391.

Genkov T, Spreitzer RJ. 2009. Highly conserved small subunit residues influence Rubisco large subunit catalysis. The Journal of Biological Chemistry **284**, 30105–30112.

Getzoff TP, Zhu G, Bohnert HJ, Jensen RG. 1998. Carboxylase / oxygenase containing a pea small subunit protein is compromised in carbamylation. Plant Physiology **116**, 695–702.

Hahn F, Nekrasov V. 2019. CRISPR/Cas precision: do we need to worry about off-targeting in plants Plant Cell Reports **38**, 437–441.

Hoshino R, Yoshida Y, Tsukay H. 2019. Multiple steps of leaf thickening during sun-leaf formation in Arabidopsis. The Plant Journal **100**, 738–753.

Howe CJ, Auffret AD, Doherty A, Bowman CM, Dyer TA, Gray JC. 1982. Location and nucleotide sequence of the gene for the proton-translocating subunit of wheat chloroplast ATP synthase. Proceedings of the National Academy of Sciences USA **79**, 6903–6907.

Hug N, Longman D, Cáceres JF. 2015. Mechanism and regulation of the nonsense-mediated decay pathway. Nucleic Acids Research **44**, 1483–1495.

Ishida H, Yoshimoto K, Izumi M, Reisen, D, Yano Y, Makino A, Ohsumi Y, Hanson MR, Mae T. 2008. Mobilization of Rubisco and stroma-localized fluorescent proteins of

582 chloroplasts to the vacuole by an ATG gene-dependent autophagic process. Plant
583 Physiology **148**, 142–155.

584 **Ishikawa C, Hatanaka T, Misoo S, Miyake C, Fukayama H**. 2011. Functional
585 incorporation of sorghum small subunit increases the catalytic turnover rate of Rubisco
586 in transgenic rice. Plant Physiology **156**, 1603–11.

587 **Izumi M, Tsunoda H, Suzuki Y, Makino A, Ishida H**. 2012. RBCS1A and RBCS3B, two
588 major members within the Arabidopsis RBCS multigene family, function to yield
589 sufficient Rubisco content for leaf photosynthetic capacity. Journal of Experimental
590 Botany **63**, 2159–2170.

591 **Khumsupan P, Donovan S, McCormick AJ**. 2019. CRISPR/Cas in Arabidopsis:
592 overcoming challenges to accelerate improvements in crop photosynthetic efficiencies.
593 Physiologia Plantarum **166**, 428–437.

594 **Klepikova AV, Kasianov AS, Gerasimov ES, Logacheva MD, Penin AA**. 2016. A high
595 resolution map of the *Arabidopsis thaliana* developmental transcriptome based on RNA-
596 seq profiling. The Plant Journal **88**, 1058–1070.

597 **Kostov RV, Small CL, McFadden BA**. 1997. Mutations in a sequence near the N-terminus
598 of the small subunit alter the CO_2/O_2 specificity factor for ribulose bisphosphate
599 carboxylase/oxygenase. Photosynthesis Resesearch **54**, 127–134.

600 **Krebbers E, Seurinck J, Herdies L, Cashmore AR, Timko MP**. 1988. Four genes in two
601 diverged subfamilies encode the ribulose-1,5-bisphosphate carboxylase small subunit
602 polypeptides of *Arabidopsis thaliana*. Plant Molecular Biology **11**, 745–759.

603 **Kubis A, Bar-Even A**. 2019. Synthetic biology approaches for improving photosynthesis.
604 Journal of Experimental Botany **70**, 1425–1433.

605 **Laterre R, Pottier M, Remacle C, Boutry M**. 2017. Photosynthetic trichomes contain a
606 specific Rubisco with a modified pH-dependent activity. Plant Physiology **173**, 2110–
607 2120.

608 **Li J, Chory J**. 1998. Preparation of DNA from Arabidopsis. Methods in Molecular Biology
609 **82**, 55–60.

610 **Li W, Teng F, Li T, Zhou Q**. 2013. Simultaneous generation and germline transmission of

611 multiple gene mutations in rat using CRISPR-Cas systems. Nature Biotechnology **31**,
612 684–686.

613 **Liang G, Zhang H, Lou D, Yu D**. 2016. Selection of highly efficient sgRNAs for CRISPR/
614 Cas9-based plant genome editing. Scientific. Reports **19**, 1–8.

615 **Lin MT, Stone WD, Chaudhari V, Hanson MR**. 2019. Enzyme kinetics of tobacco
616 Rubisco expressed in *Escherichia coli* varies depending on the small subunit
617 composition. BioRxiv (doi: https://doi.org/10.1101/562223).

618 **Maxwell K, Johnson GN**. 2000. Chlorophyll fluorescence - A practical guide. Journal of
619 Experimental Botany **51**, 659–668.

620 **McCormick AJ, Kruger NJ**. 2015. Lack of fructose 2,6-bisphosphate compromises
621 photosynthesis and growth in Arabidopsis in fluctuating environments. The Plant
622 Journal **81**, 670–683.

623 **Meier I, Callan KL, Fleming AJ, Gruissem W**. 1995. Organ-specific differential regulation
624 of a promoter subfamily for the ribulose-1,5-bisphosphate carboxylase/oxygenase small
625 subunit genes in tomato. Plant Physiology **107**, 1105–1118.

626 **Morita K, Hatanaka T, Misoo S, Fukayama H**. 2014. Unusual small subunit that is not
627 expressed in photosynthetic cells alters the catalytic properties of Rubisco in rice. Plant
628 Physiology **164**, 69–79.

629 **Nacry P, Camilleri C, Courtial B, Caboche M, Bouchez D**. 1998. Major chromosomal
630 rearrangements induced by T-DNA transformation in Arabidopsis. Genetics **149**, 641–
631 650.

632 **Nagaya S, Kawamura K, Shinmyo A, Kato K**. 2010. The HSP terminator of *Arabidopsis*
633 *thaliana* increases gene expression in plant cells. Plant and Cell Physiology **51**, 328–
634 332.

635 **Niwa Y, Goto K, Shimizu M, Kobayashi H**. 1997. Chromosomal mapping of genes in the
636 *RBCS* family in *Arabidopsis thaliana*. DNA Research **4**, 341–343.

637 **Ogawa S, Suzuki Y, Yoshizawa R, Kanno K, Makino A**. 2012. Effect of individual
638 suppression of *RBCS* multigene family on Rubisco contents in rice leaves. Plant, Cell
639 and Environment **35**, 546–553.

Orr DJ, Worrall D, Lin MT, Carmo-Silva E, Hanson MR, Parry MAJ. 2019. Hybrid cyanobacterial-tobacco Rubisco supports autotrophic growth and pro-carboxysomal aggregation. Plant Physiology doi: 10.1104/pp.19.01193.

Parry G, Patron N, Bastow R, Matthewman C. 2016. Meeting report: GARNet/OpenPlant CRISPR-Cas workshop. Plant Methods **12**, 1–7.

Patron N, Orzaez D, Marillonnet S et al. 2015. Standards for plant synthetic biology: a common syntax for exchange of DNA parts. New Phytologist **1**, 13–19.

Paul K, Morell MK, Andrews TJ. 1991. Mutations in the small subunit of ribulose bisphosphate carboxylase affect subunit binding and catalysis. Biochemistry **30**, 10019–10026.

Pauwels L, De Clercq R, Goossens J, Iñigo S, Williams C, Ron M, Britt A, Goossens A. 2018. A Dual sgRNA approach for functional genomics in *Arabidopsis thaliana*. G3: Genes, Genomes, Genetics **8**, 2603–2615.

Porra RJ, Thompson WA, Kriedemann PE. 1989. Determination of accurate extinction coefficients and simultaneous-equations for assaying chlorophyll-a and chlorophyll-b extracted with 4 different solvents - verification of the concentration of chlorophyll standards by atomic-absorption spectroscopy. Biochimica et Biophysica Acta **975**, 384–394.

Pottier M, Gilis D, Boutry M. 2018. The hidden face of Rubisco. Trends in Plant Science **23**, 382–392.

Qiu Y, Tay Y, Van Ruan Y, Adams KL. 2019. Divergence of duplicated genes by repeated partitioning of splice forms and subcellular localization. New Phytologist **225**, 1011–1022.

Quick WP, Schurr U, Scheibe R, Schulze ED, Rodermel SR, Bogorad L, Stitt M. 1991. Decreased ribulose-1,5-bisphosphate carboxylase-oxygenase in transgenic tobacco transformed with "antisense" *rbcS* - I. Impact on photosynthesis in ambient growth conditions. Planta **183**, 542–554.

Rae BD, Long BM, Förster B, Nguyen ND, Velanis CN, Atkinson N, Hee WY, Mukherjee B, Price GD, McCormick AJ. 2017. Progress and challenges of

engineering a biophysical CO_2-concentrating mechanism into higher plants. Journal of Experimental Botany **68**, 3717–3737.

Raitskin O, Schudoma C, West A, Patron NJ. 2019. Comparison of efficiency and specificity of CRISPR-associated (Cas) nucleases in plants: An expanded toolkit for precision genome engineering. PLoS One **14**, 1–17.

Read BA, Tabita FR. (1992) A hybrid ribulosebisphosphate carboxylase/oxygenase enzyme exhibiting a substantial increase in substrate specificity factor. Biochemistry **31**, 5553–5560.

Rodermel S. 1999. Subunit control of Rubisco biosynthesis – a relic of an endosymbiotic past. Photosynthesis Research **59**, 105–123.

Rodermel S, Haley J, Jiang CZ, Tsai CH, Bogorad L. 1996. A mechanism for intergenomic integration: abundance of ribulose bisphosphate carboxylase small-subunit protein influences the translation of the large-subunit mRNA. Proceedings of the National Academy of Sciences USA **93**: 3881–3885.

Sasanuma, T. 2001. Characterization of the *rbcS* multigene family in wheat: subfamily classification, determination of chromosomal location and evolutionary analysis. Molecular Genetics and Genomics **265**, 161–171.

Sawchuk MG, Donner TJ, Head P, Scarpella E. 2008. Unique and overlapping expression patterns among members of photosynthesis-associated nuclear gene families in Arabidopsis. Plant Physiology **148**, 1908–1924.

Schneider G, Knight S, Andersson I, Brändén CI, Lindqvist Y, Lundqvist T. 1990. Comparison of the crystal structures of L2 and L8S8 Rubisco suggests a functional role for the small subunit. EMBO Journal **9**, 2045–2050.

Schwarte S, Tiedemann R. 2011. A gene duplication/loss event in the ribulose-1, 5-bisphosphate-carboxylase/oxygenase (Rubisco) small subunit gene family among accessions of *Arabidopsis thaliana*. Molecular Biology and Evolution **28**, 1861–1876.

Sharwood RE, Sonawane BV, Ghannoum O, Whitney SM. 2016. Improved analysis of C4 and C3 photosynthesis via refined in vitro assays of their carbon fixation biochemistry. Journal of Experimental Botany **67**, 3137–3148.

Shimada TL, Shimada T, Hara-Nishimura I. 2010. A rapid and non-destructive screenable marker, FAST, for identifying transformed seeds of *Arabidopsis thaliana*. The Plant Journal **61**, 519–528.

Simkin AJ, López-Calcagno PE, Raines CA. 2019. Feeding the world: improving photosynthetic efficiency for sustainable crop production. Journal of Experimental Botany **70**, 1119–1140.

South PF, Cavanagh AP, Liu HW, Ort DR. 2019. Synthetic glycolate metabolism pathways stimulate crop growth and productivity in the field. Science **363**, 1–10.

Spreitzer RJ, Peddi SR, Satagopan S. 2005. Phylogenetic engineering at an interface between large and small subunits imparts land-plant kinetic properties to algal Rubisco. Proceedings of the National Academy of Sciences USA **102**, 17225–30.

Suzuki Y, Nakabayashi K, Yoshizawa R, Mae T, Makino A. 2009. Differences in expression of the *RBCS* multigene family and Rubisco protein content in various rice plant tissues at different growth stages. Plant and Cell Physiology **50**, 1851–1855.

Valegård K, Hasse D, Andersson I, Gunn LH. 2018. Structure of Rubisco from *Arabidopsis thaliana* in complex with 2-carboxyarabinitol-1,5-bisphosphate. Acta Crystallographica Section D: Structural Biology **74**, 1–9.

van Lun M, van der Spoel D, Andersson I. 2011. Subunit interface dynamics in hexadecameric Rubisco. Journal of Molecular Biology **411**, 1083–1098.

Vasudevan R, Gale GAR, Schiavon AA, Puzorjov A, Malin J, Gillespie MD, Vavitsas K, Zulkower V, Wang B, Howe CJ, Lea-Smith DJ, McCormick AJ. 2019. Cyanogate: A modular cloning suite for engineering cyanobacteria based on the plant MoClo syntax. Plant Physiology **180**, 39–55.

Wanner LA, Gruissem W. 1991. Expression dynamics of the tomato *rbcS* gene family during development. The Plant Cell **3**, 1289–303.

Wehmeyer B, Cashmore AR, Schäfer E. 1990. Photocontrol of the expression of genes encoding chlorophyll a/b binding proteins and small subunit of ribulose-1,5-bisphosphate carboxylase in etiolated seedlings of *Lycopersicon esculentum* (L.) and *Nicotiana tabacum* (L.). Plant Physiology **93**, 990–997.

Whitney SM, Birch R, Kelso C, Beck JL, Kapralov MV. 2015. Improving recombinant Rubisco biogenesis, plant photosynthesis and growth by coexpressing its ancillary RAF1 chaperone. Proceedings of the National Academy of Sciences USA **112**, 3564–3569.

Wolter F, Schindele P, Puchta H. 2019. Plant breeding at the speed of light: The power of CRISPR/Cas to generate directed genetic diversity at multiple sites. BMC Plant Biology **19**, 1–8.

Wostrikoff K, Clark A, Sato S, Clemente T, Stern D. 2012. Ectopic expression of Rubisco subunits in maize mesophyll cells does not overcome barriers to cell type-specific accumulation. Plant Physiology **160**, 419–432.

Wostrikoff K, Stern D. 2007. Rubisco large-subunit translation is autoregulated in response to its assembly state in tobacco chloroplasts. Proceedings of the National Academy of Sciences USA **104**, 6466–6471.

Yamada K, Davydov II, Besnard G, Salamin N. 2019. Duplication history and molecular evolution of the *rbcS* multigene family in angiosperms. Journal of Experimental Botany **70**, 6127–6139.

Yoon M, Putterill JJ, Ross GS, Laing WA. 2001. Determination of the relative expression levels of rubisco small subunit genes in Arabidopsis by rapid amplification of cDNA ends. Analytical Biochemistry **291**, 237–244.

Figure Legends

Figure 1. The Rubisco small subunit gene family in *Arabidopsis thaliana*. (A) The sites of the T-DNA insertions for mutant lines used in this study are shown in blue with the orientation of the left border (LB) indicated. The locations targeted by CRISPR-Cas9 are shown, with the names of the targeting gRNAs in green boxes (see Table S1 and vector maps in Data S1 for gRNA sequences). The 5' and 3' untranslated regions (UTR) are shown for each gene. (B) The B subfamily is located in tandem in the 1B-3B locus. A promiscuous pair of gRNAs targeting the three small subunits in the 1B-3B locus is indicated.

Figure 2. Targeted mutagenesis of Rubisco small subunits in protoplasts of *Arabidopsis thaliana* using vectors encoding Cas9 and gRNA pairs. (A) Detection of mutations using PCR. Lane 1, DNA marker; Lanes 2 - 9, PCR products of genomic DNA from protoplasts transfected with vectors carrying gRNA pairs targeting Rubisco small subunit (SSU) genes *1A* (1AP1, 1AP2), *1B* (1BP1, 1BP2), *2B* (2BP1, 2BP2) and *3B* (3BP1, 3BP2) (see Table S2 for primer details). (B) Sequencing results of the lower "deletion band" showed deletions events 3-4 bp upstream of the PAM site (underlined). The gRNA target sequences are shown in bold.

Figure 3. Total soluble protein and Rubisco contents in *rbcs* mutants of *Arabidopsis thaliana*. (A) The *1a2b3b* mutant compared to *1a3b* and WT plants grown under standard conditions. All images represent 28-d-old rosettes unless otherwise stated. (B) Total soluble protein content shown for 35-d-old plants. (C**)** Rubisco content determined by ^{14}C-CABP binding and subunit ratios estimated by immunoblotting. Values are means ± SE of five measurements. (D) Representative immunoblots of *rbcs* mutants probed with a serum containing polyclonal antibodies against Rubisco to illustrate the reduction or absence of each SSU subfamily. The LSU (55 kDa) and SSU (14.7 kDa for 1A and 14.8 kDa for the B subfamily) are shown. See Table S5 for further results and statistical analysis.

Figure 4. Growth phenotypes of *rbcs* mutants of *Arabidopsis thaliana* grown under standard and high light conditions. (A) Rosette area expansion of *rbcs* single T-DNA an CRISPR/Cas9 (CC) mutants, (B) rosette area expansion of double and triple mutants (the insert shows the expansion of *1a2b3b* at appropriate scale), and (C) fresh and dry weights of 28-d-old rosettes of all mutant lines grown under standard conditions. (D) Rosette area expansion of *1b*, *2b* and *3b* T-DNA and CRISPR/Cas9 mutants, (E) rosette area expansion of *1a*, *2b3b*, *1a2b* and *1a3b* mutants, and (F) fresh and dry weights of 28-d-old rosettes for all mutant lines grown under high light conditions. (G) Representative examples of 20-d-old rosettes of plants grown standard conditions and (H) under high light conditions. Letters in the legends for (B) and (E) indicate significant difference between plant lines ($P < 0.05$) as determined by repeated measures ANOVA followed by Tukey's HSD tests. See Table S6 for further results and statistical analysis.

Figure 5. Photosynthetic CO_2 response curves of *rbcs* mutants of *Arabidopsis thaliana*. Measurements were made on fully expanded sixth or seventh leaf of 35- to 45-d-old non-flowering rosettes for WT and mutants and 80-d-old non-flowering rosettes for *1a2b3b*. The A/C_i curves show the response of net CO_2 assimilation (A) to different sub-stomatal concentration of CO_2 (C_i) under saturating light (1,800 µmol photon m^{-2} s^{-1}) for A) *1b* and *2b* mutants, B) *1a* and *3b* mutants, and C) *2b3b*, *1a2b*, *1a3b*, and *1a2b3b* mutants. Each value represents the means ± SE of measurements made on individual leaves from three to four different rosettes.

Table 1. Editing efficiency of paired gRNAs targeting each *rbcS* gene. T1 plants containing Cas9 were screened by PCR for large deletions and Sanger sequencing for indels and point mutations (PMs). T1 lines containing large deletions or indels/PMs were screened for heritable mutations in Cas9-free plants in the T2 generation. Six of Cas9-free T2 plants were sequenced for each T1 line (34 lines for 1AP2, 11 lines for 1BP2, 13 for 2BP2, 11 lines for 3BP1 and 8 lines for 1B3B).

gRNA pair	Target gene	Background	Number of T1 plants (with transgene)		Number of T2 plants (Transgene-free)	
			Large deletion	Indels/PM	Large deletion	Indels/PM
1AP2	1A	WT	8/92 (9%)	26/106 (25%)	0/8 (0%)	24/204 (12%)
1BP2	1B		0/112 (0%)	11/35 (31%)	N/A	42/66 (64%)
2BP2	2B		1/69 (1%)	12/63 (19%)	0/1 (0%)	30/78 (38%)
3BP1	3B		10/70 (14%)	1/32 (3%)	0/10 (0%)	24/66 (36%)
1B3B	1B	WT	8/76 (11%)	N/A	0/8 (0%)	0/64 (0%)
	2B					1/64 (2%)
	3B					8/64 (13%)
1BP2	1B	*1a2b*	0/33 (0%)	8/33 (24%)	N/A	N/A
3BP2	3B	*1a2b*	0/30 (0%)	3/30 (10%)	N/A	N/A

Table 2. Variables derived from photosynthetic CO_2 response curves, based on leaf gas exchange analysis. Values are means ± SE of measurements made on three or four leaves from different plants (35- to 45-d-old non-flowering rosettes for WT and mutants and 80-d-old non-flowering rosettes for *1a2b3b*). Values followed by the same letters in the same column are not significantly different ($P < 0.05$) as determined by ANOVA followed by Tukey's HSD tests. Abbreviations: Γ, sub-stomatal CO_2 compensation point; g_s, stomatal conductance at 400 ppm CO_2; R_d, mitochondrial respiration in the light; V_{cmax}, maximum rate of Rubisco carboxylation.

	V_{cmax} (μmol CO_2 m^{-2} s^{-1})	R_d (μmol CO_2 m^{-2} s^{-1})	g_s (mmol H_2O m^{-2} s^{-1})	Γ (μmol CO_2 mol^{-1})
WT	55.5 ± 3.5 ^{a}	1.01 ± 0.27 ^{a}	0.25 ± 0.03 ^{a}	52.4 ± 4.7 ^{a}
1a T-DNA	38.0 ± 3.2 ^{bc}	1.18 ± 0.11 ^{a}	0.20 ± 0.03 ^{a}	65.7 ± 10.1 ^{ab}
1a CC1	38.1 ± 2.0 ^{bc}	0.93 ± 0.08 ^{a}	0.25 ± 0.01 ^{a}	61.3 ± 1.0 ^{ab}
1b T-DNA	50.3 ± 5.2 ^{ab}	1.20 ± 0.11 ^{a}	0.24 ± 0.01 ^{a}	63.2 ± 3.2 ^{ab}
1b CC1-3	49.4 ± 1.4 ^{ab}	0.83 ± 0.08 ^{a}	0.28 ± 0.01 ^{a}	53.8 ± 1.3 ^{a}
2b T-DNA	48.2 ± 4.7 ^{ab}	1.17 ± 0.08 ^{a}	0.24 ± 0.07 ^{a}	60.1 ± 2.3 ^{ab}
2b CC1-3	48.9 ± 1.5 ^{ab}	0.81 ± 0.06 ^{a}	0.28 ± 0.02 ^{a}	52.7 ± 1.3 ^{a}
3b T-DNA	39.8 ± 2.0 ^{b}	0.73 ± 0.05 ^{a}	0.26 ± 0.01 ^{a}	52.5 ± 0.8 ^{a}
3b CC1-3	38.5 ± 1.5 ^{bc}	0.77 ± 0.03 ^{a}	0.27 ± 0.01 ^{a}	54.7 ± 2.4 ^{a}
2b3b	36.9 ± 3.2 ^{bc}	0.85 ± 0.07 ^{a}	0.25 ± 0.02 ^{a}	65.3 ± 2.9 ^{ab}
1a2b	36.3 ± 2.9 ^{bc}	0.78 ± 0.08 ^{a}	0.27 ± 0.01 ^{a}	64.7 ± 2.3 ^{ab}
1a3b	24.6 ± 1.0 ^{c}	0.71 ± 0.04 ^{a}	0.26 ± 0.01 ^{a}	70.0 ± 1.5 ^{b}
1a2b3b	5.4 ± 0.3 ^{d}	0.84 ± 0.13 ^{a}	0.23 ± 0.04 ^{a}	200.1 ± 3.8 ^{c}

Figure 1

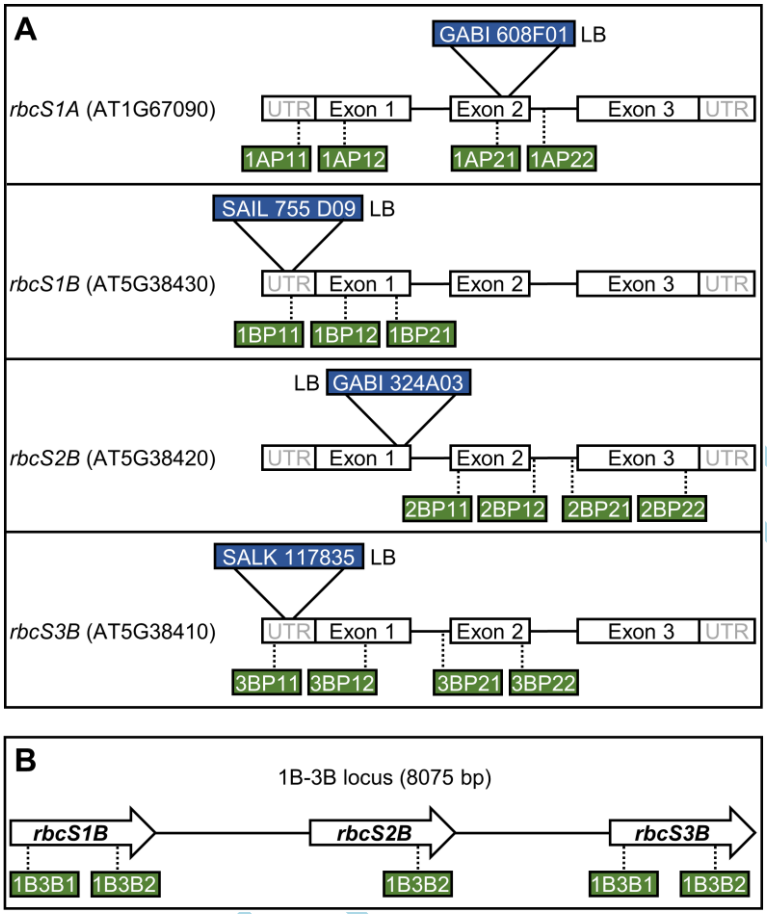

Figure 2

A

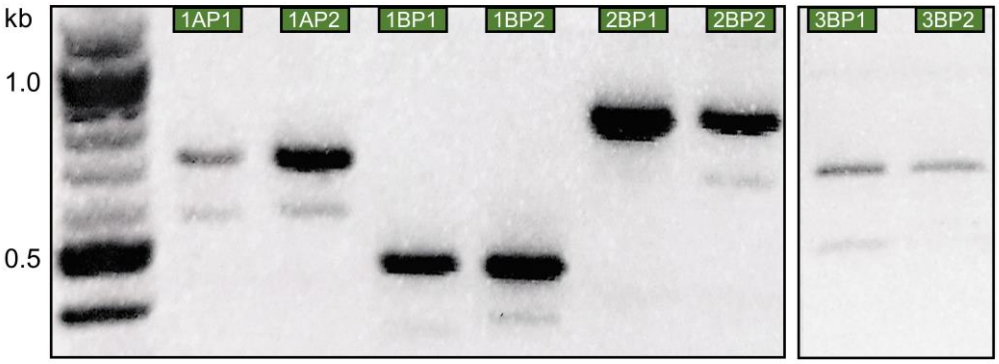

B

1AP1

TGTATCCT**AGACCCTCCGATCACTCCAA [130 bp] TATGCTCTCTTCCGCTACTA**TGGTTGCCT

TGTATCCT**AGA**----------**CTA**TGGTTGCCT

1AP2

TCTTACCT**TCCTGACCTTACCGATTCCG [126 bp] ATATAAACTAGCTAGATCTT**AGGAAAATT

TCTTACCT**TCC**----------**TCTT**AGGAAAATT

1BP1

GCTCTCCT**CTGCCGCTGTGGTTACCTCC [119 bp] TTACTTCCATCACAAGCAAT**GGGGGAAG

GCTCTCCT**CTG**----------**AAT**GGGGGAAG

1BP2

TTTTGCCT**CTTACGGTTCTCACTATATA [96 bp]** CCT**CTGCCGCTGTGGTTACCTCC**CCGGC

TTTTGCCT**CTTA**----------**CCGCTGTGGTTACCTCC**CCGGC

2BP2

CAATA**TATATATCAATTGTATTGAA**TGG **[168 bp]** CCC**TGGCGCCTTCATTAGGATCA**TCGGA

CAATA**TATATATCAATTGTATT**----------**CGCCTTCATTAGGATCA**TCGGA

3BP1

ATTAT**ATAAAGATGACAACACCAGT**AGG **[180 bp] GGTCACCCGCAAGACCAACA**AGGACATC

ATTATATAAAGATGACAACACC----------**AACA**AGGACATC

Figure 3

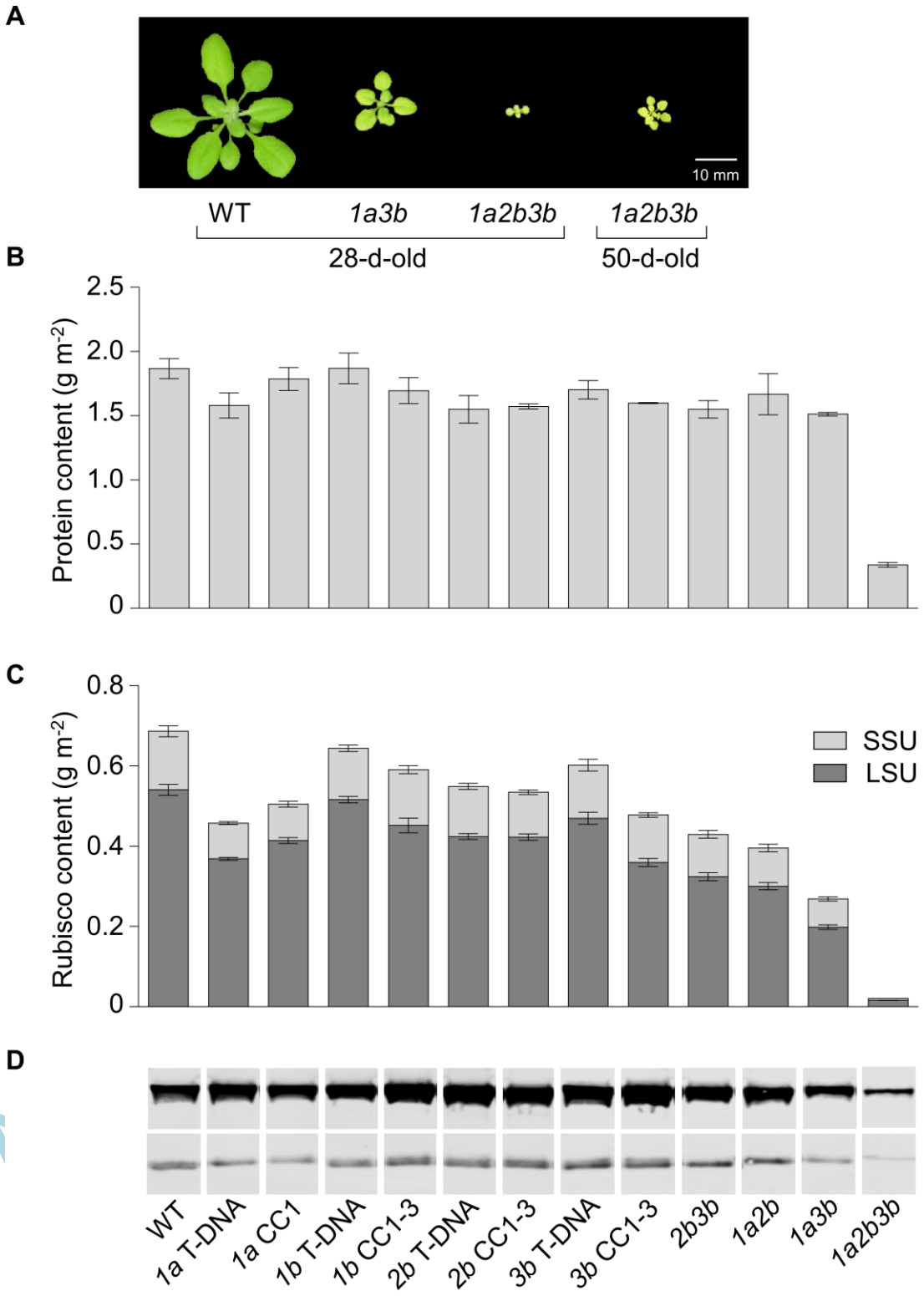

Figure 4

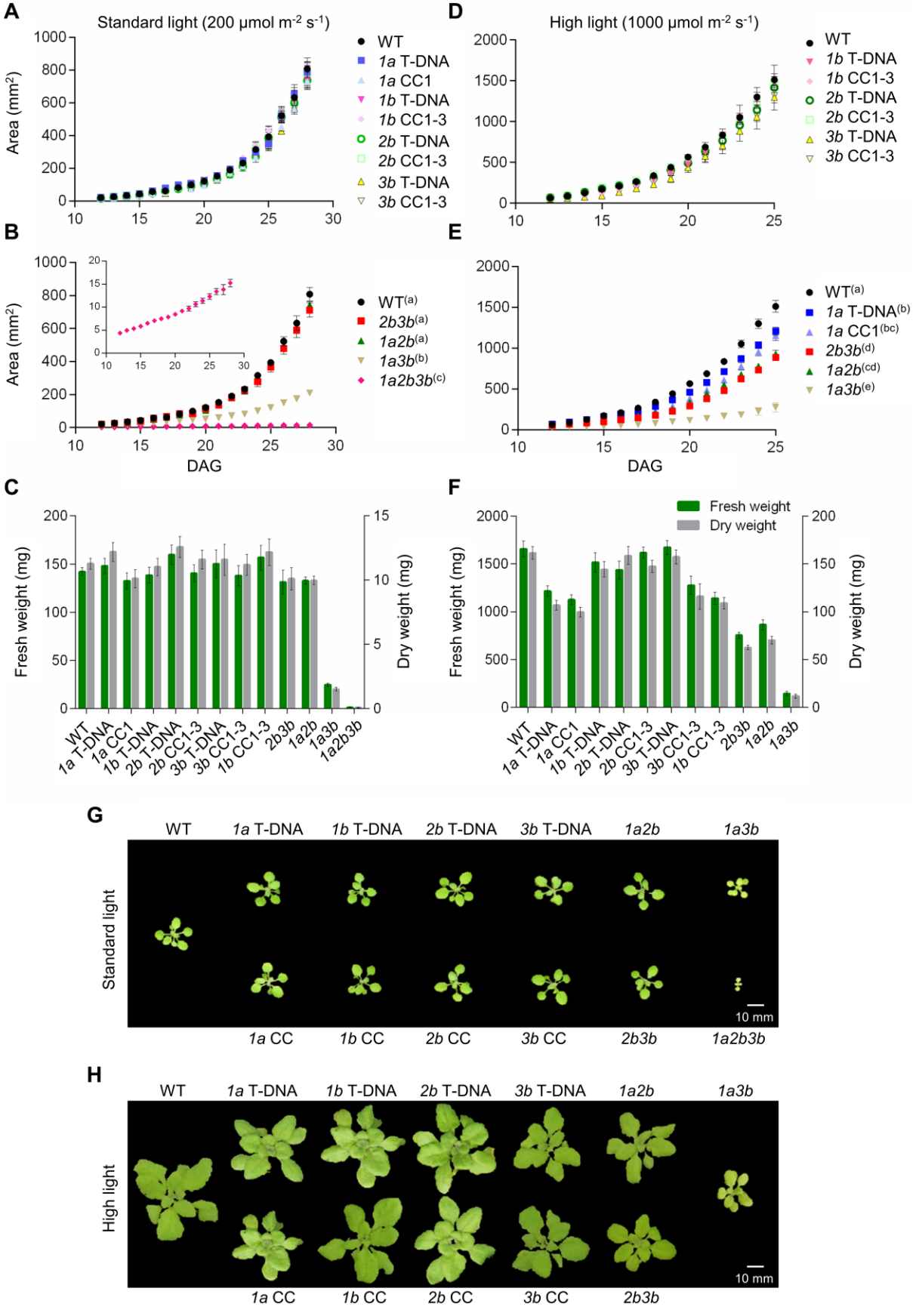

Figure 5